Calculation Models for Grounding Systems Based on Hybrid Methods

J. Meppelink
University of Applied Sciences, Soest, Germany
Tel: +49 02921378308 - janmeppelink@mac.com

R. Andolfato, D. Cuccarollo
SINT Ingegneria Srl, Italy
Tel: +39 0424568457 - r.andolfato@sintingegneria.it - d.cuccarollo@sintingegneria.it

Abstract

This paper analyzes the calculation models employed by two commercial grounding system analysis modules, GSA® and GSA_FD® which are included in the XGSLab® software.
GSA® considers only equipotential electrodes, whereas GSA_FD® considers both voltage drop along the self-impedance and mutual impedance effects.
The comparison is carried out by taking into account grounding grids with sizes in the range 50 m x 50 m and 600 m x 600 m, soil resistivity in the range 1 Ω·m and 10 kΩ·m, and frequency in the range 1 Hz and 1 MHz.
Despite the fact that both of the modules can consider uniform and double layer soil models, the analysis is carried out only for the uniform soil model case. As well known, most of the soils are not uniform, but this hypothesis allows a reduction of parameters number and consequently obtaining results of practical use.
Moreover, the analysis considers only copper-made grids because copper is the most widely used material for grounding systems. Steel use is also widespread, but because of the higher resistivity and magnetic permeability compared to copper, steel-made grids required a specific study that should be discussed in a separate paper.
The considered parameters are then grid size, soil resistivity and frequency. The scope of this paper is to investigate when GSA® may be used and consequently, when GSA_FD® should be used.
Key words
Computer modelling; PEEC; EMC; grounding design.

1.   Introduction

The large improvement of power computing performances is contributing to the diffusion of calculation programs for grounding system analysis.
The first generation of these programs was based on the hypothesis of equipotential electrodes (e.g. CYMGRD®, ETAP®, GSA®, MALT®).
The second generation eliminated the equipotential condition hypothesis and investigated the voltage drop along the self-impedance of the conductors, but ignored the mutual impedance effects (e.g. MALZ®).
The third generation, it also considers the mutual impedance effects (e.g. GSA_FD®, HIFREQ®).
In the following paper, the commercial programs GSA® and GSA_FD® are examined, but the conclusions are useful for all programs that are based on a similar model.
GSA® has been validated by comparison with measured values, using analytical cases and results published in the IEEE Std. 80-2013, whereas GSA_FD® has been validated by comparison with MALZ® when the mutual impedance is ignored, and with HIFREQ® when the mutual impedance is taken into account. MALZ® and HIFREQ® are well established commercial modules included in the CDGES® software which were assumed as accepted reference. The validation reports are included in the XGSLab® Tutorial and are available on request.
The agreement between XGSLab® and CDGES® results is an important starting point for this work and on the other hand, it represents a further validation of the "shifting complex images method" [9] implemented in XGSLab®.
For simplicity, in the following paper GSA® is referred to as model A and GSA_FD® is referred to as both model B when the mutual impedance is ignored, and model C when the mutual impedance is taken into account.
The main assumptions of the three models are listed in Table 1.1.
A similar parametric study limited to the power frequency was proposed in [11] and in this paper this analysis is completed and extended to the frequency range 1 Hz - 1 MHz.

Aspects taken into account	Model A	Model B	Model C
Resistive Coupling	Yes	Yes	Yes
Capacitive Coupling	No	Yes	Yes
Self-Impedance	No	Yes	Yes
Mutual Impedance	No	No	Yes

Table 1.1. Aspects taken into account in the three models.

2.   Calculation Models

Calculation models for grounding systems analysis may be based on following different approaches: 1) Electromagnetic field theory; 2) Transmission line theory; 3) Hybrid methods, 4) Circuit theory. This classification is not rigorous as indicated in [10], but is generally adopted in the literature although recently hybrid methods are often called PEEC (Partial Element Equivalent Circuit) methods. For a comprehensive overview on computational methods for grounding systems refer to [10].
Hybrid methods consider transmission line, circuit and electromagnetic field theory combined into a single model, and are often preferred in the frequency range of interest (up to a few MHz). Hybrid methods are very useful for an engineering purpose because they are accurate and flexible, and can allow an easy way to consider additional external parameters such as electromotive forces, currents, and

impedances. Hybrid methods may be used at low frequency [4] and also at high frequency [14].

All three investigated models A, B and C are based on hybrid methods. The grounding system is partitioned into a suitable number of finite elements and then, the electromagnetic field and transmission line theories are used to calculate the circuit parameters, whereas circuit theory is employed to describe the relations among parameters such as voltages and currents and the metallic connections among elements.

With more details, the method used in the investigated models is described in the following.

The method derives directly from the Maxwell equations. Using the scalar and vector potentials, Maxwell equations can be written as in the following (Helmholtz equations):

$$\begin{cases} \Delta \dot{\mathbf{A}} - \dot{\gamma}^2 \dot{\mathbf{A}} = -\mu \dot{\mathbf{J}} \\ \Delta \dot{V} - \dot{\gamma}^2 \dot{V} = -\dfrac{\dot{q}}{\varepsilon} \end{cases} \quad (1)$$

where $\dot{\gamma} = \sqrt{j\omega\mu(\sigma + j\omega\varepsilon)}$ represents the propagation coefficient of the medium and $\dot{q}$ and $\dot{J}$ represent charge and current density distribution on the sources respectively. Solution of (1) for sources with linear current and charge density distribution are given by the following equations:

$$\begin{cases} \dot{\mathbf{A}} = \dfrac{\mu}{4\pi} \int_L \dot{I} \dfrac{e^{-\dot{\gamma}r}}{r} dl \\ \dot{V} = \dfrac{1}{4\pi\dot{\varepsilon}} \int_L \dot{q} \dfrac{e^{-\dot{\gamma}r}}{r} dl \end{cases} \quad (2)$$

Maxwell equations give the following well known relation between electric field and scalar and vector potentials:

$$\dot{\mathbf{E}} = -grad\dot{V} - j\omega\dot{\mathbf{A}} \quad (3)$$

Taking into account that the electric field and vector potential on the surface of a conductor are parallel to the conductor axis [4], only the magnitude of vectors in (3) need to be considered and (3) written along the conductor axis gives:

$$\dot{E} = -\dfrac{\partial \dot{V}}{\partial l} - j\omega\dot{A} \quad (4)$$

On the other hand, the tangential electric field on the surface of a conductor, taking into account their self impedance, gives:

$$\dot{E} = \dot{z}\dot{I} \quad (5)$$

Combining (4) and (5), the following fundamental differential equation is obtained:

$$\dot{z}\dot{I} + j\omega\dot{A} + \dfrac{\partial \dot{V}}{\partial l} = 0 \quad (6)$$

Equation (6) is derived directly from the Maxwell equations

and is then valid in all conditions (also non stationary).

In practical cases, (6) can be solved only in a numerical way.

The system of conductors is then partitioned into a suitable number of short elements.

Each element is oriented between its start point (in) and its end point (out).

Integrating (6) between the ends of an element, replacing the vector and scalar potential with (2) and rearranging, the following linear equation is obtained:

$$\dot{Z}_i \dot{I}_i + \sum_{j \neq i} \dot{M}_{ij} \dot{I}_j + \sum \left(\dot{w}_{outij} - \dot{w}_{inij} \right) \dot{J}_j = 0 \quad (7)$$

with:

$$\dot{M}_{ij} = \dfrac{j\omega\mu}{4\pi} \int_{in}^{out} \int_{in}^{out} \dfrac{e^{-\dot{\gamma}r}}{r} dl_i dl_j \quad (7a)$$

$$\dot{w}_{outij} = \dfrac{\dot{\rho}}{4\pi d} \int_{in}^{out} \dfrac{e^{-\dot{\gamma}r}}{r} dl_j \bigg|_{out} \quad (7b)$$

$$\dot{w}_{inij} = \dfrac{\dot{\rho}}{4\pi d} \int_{in}^{out} \dfrac{e^{-\dot{\gamma}r}}{r} dl_j \bigg|_{in} \quad (7c)$$

and where $\dot{Z}$ represents the self impedance of the element, $\dot{M}$ and $\dot{w}$ represent mutual coupling and potential coefficient between elements respectively and $\dot{I}$ and $\dot{J}$ represent longitudinal and leakage current respectively.

Writing a linear equation for each element, the Maxwell equation are then reduced to a linear system.

For the calculation of the linear system coefficients and then of the mutual coupling and potential coefficients between elements, the shifting complex images method (SCIM) [9] and the modified images method (MIM) [7] has been used respectively.

Each element is represented with a simplified equivalent circuit as shown in Fig. 2.1 and introduces the following unknowns:
- Input and Output currents I_{in} and I_{out}
- Leakage current J
- Potential V of the middle point
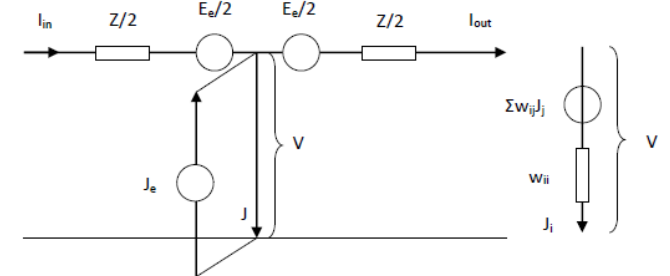
Fig. 2.1. Equivalent circuit of each element.

The linear systems to calculate the unknowns are more or less complex depending on the adopted model, as follows:

Model A:
$$\begin{cases} \{V\} = [W]\{J\} \\ \sum J = J_e \ \forall \ electrode \end{cases} \quad (8)$$

2

Model B:

$$\begin{cases} \{V\} = [W]\{J\} \\ \{E_z\} + \{E_e\} = -[Z]\{I\} \\ \{J\} = [A]\{I\} + \{J_e\} \end{cases} \qquad (9)$$

Model C:

$$\begin{cases} \{V\} = [W]\{J\} \\ \{E_z\} + \{E_e\} = -([Z]+[M])\{I\} \\ \{J\} = [A]\{I\} + \{J_e\} \end{cases} \qquad (10)$$

where:

- $[W]$ = matrix of self and mutual potential coefficient
- $[Z]$ = matrix of self-impedances
- $[M]$ = matrix of mutual impedances
- $[A]$ = incidence matrix
- $\{V\}$ = vector of potentials
- $\{I\}$ = vector of currents
- $\{J\}$ = vector of leakage currents
- $\{E_z\}$ = vector of voltage drops
- $\{J_e\}$ = vector of injected currents
- $\{E_e\}$ = vector of forcing electromotive force

As a fundamental assumption, in model A each electrode must be considered equipotential, thus all elements are assumed to be lossless. As will be clear in the following, the equipotential condition may be assumed as valid if the maximum electrode size "D" is small compared to the wavelength "λ" of propagation in soil:

$$D << \lambda \qquad (11)$$

The wavelength propagation in soil is lower than in air and they may be calculated using the following formulae [2] [8]:

$$\lambda = 2\pi/\beta \qquad (12)$$

with, at a frequency up to several MHz:

$$\beta = \omega \sqrt{\frac{\mu_0 \varepsilon}{2}\left(\sqrt{1+\left(\frac{1}{\omega\rho\varepsilon}\right)^2}+1\right)} \cong \sqrt{\frac{\omega\mu_0}{2\rho}} \qquad (13)$$

where:
- $\omega = 2\pi f$
- f = frequency
- μ_0 = free space permeability
- ε = soil permittivity
- ρ = soil resistivity

It follows:

$$\lambda \cong 2\pi\sqrt{\frac{2\rho}{\omega\mu_0}} = 2\pi\sqrt{\frac{\rho}{\pi f \mu_0}} = 3162\sqrt{\frac{\rho}{f}} \qquad (14)$$

Model B takes into account the self-impedance, whereas model C also considers the mutual impedance. It follows, then, that both B and C models remove the main limitation of model A. However, it is not a simple task to determine their application limits.

The main aim of this paper is to research the application limits of A, B, and C models about grid size, soil resistivity and frequency. For this purpose it is required a parametric analysis.

The following Figures 2.2, 2.3, and 2.4, shown the earth surface potential applying respectively A, B, and C models to a grid 100 m x 100 m (mesh size 10 m), using a uniform soil model with resistivity 5 Ω·m and a current 10 kA, 50 Hz injected at a corner.
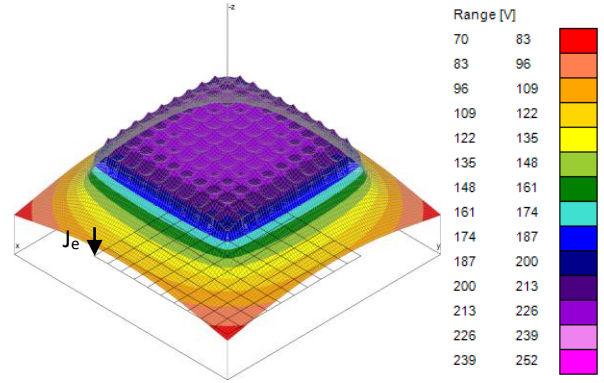
Fig. 2.2. Earth Surface Potential with model A.
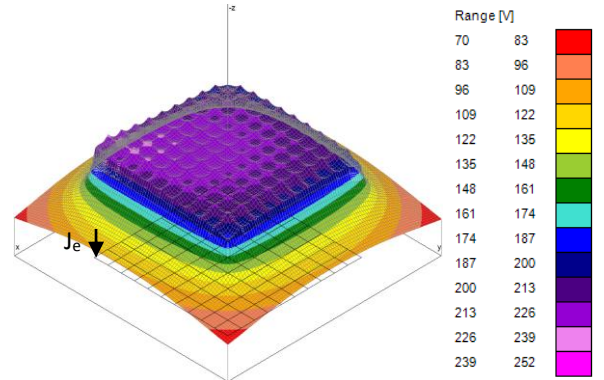
Fig. 2.3. Earth Surface Potential with model B.
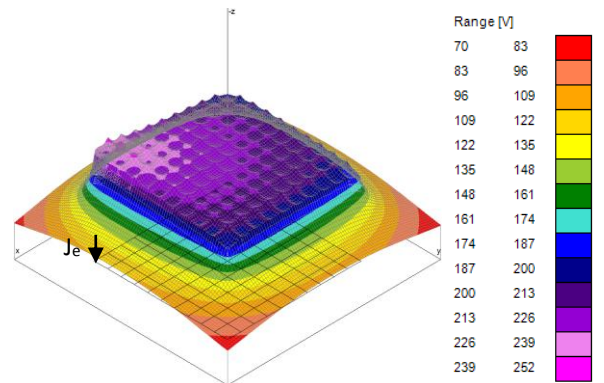
Fig. 2.4. Earth Surface Potential with model C.

A low soil resistivity value has been chosen in order to highlight the difference between the models. These figures help to clarify the behavior of an equipotential electrode (Figure 2.2) and the effects of the self (Figure 2.3) and self + mutual (Figure 2.4) impedances in qualitative manner, and are useful to better understand the results below. An

3

equipotential electrode is characterized by a quite flat distribution of the earth surface potential, with small undulations due to the mesh, while taking into account self and mutual impedances, the earth surface potential grows significantly close to the current injection point.

3. Resistivity Analysis

In the following, a 50 Hz frequency is considered.
Five grid sizes are evaluated:
- Very small grid: 50 m x 50 m with mesh size 10 m
- Small grid: 100 m x 100 m with mesh size 10 m
- Medium grid: 200 m x 200 m with mesh size 10 m
- Large grid: 400 m x 400 m with mesh size 20 m
- Very large grid: 600 m x 600 m with mesh size 30 m

The mesh sizes of the largest grids are chosen in order to reduce the calculation time but they do not affect the results of the parametric study.
In all cases, the influence of the connected leads is ignored.
The soil model is assumed as a homogeneous and isotropic half space with a plane interface with air. The soil resistivity is assumed in the range 1 – 10 kΩ·m (1, 2, 5, 10, 20, 50, 100, 200, 500, 1000, 10000 Ω·m).
In all cases, the following additional data are assumed:
- Soil relative permittivity and relative permeability are 1
- Grid depth is 0.75 m
- Current 1 kA, 50 Hz, with phase 0 deg injected in a grid corner
- Stranded copper conductors with cross section 95 mm2 and outer diameter 12.60 mm

The magnitude of the GPR values of very small, medium and very large grids are shown in the following Figures 3.1, 3.2 and 3.3 (dotted line for model A, dashed line for model B, and solid line for model C).
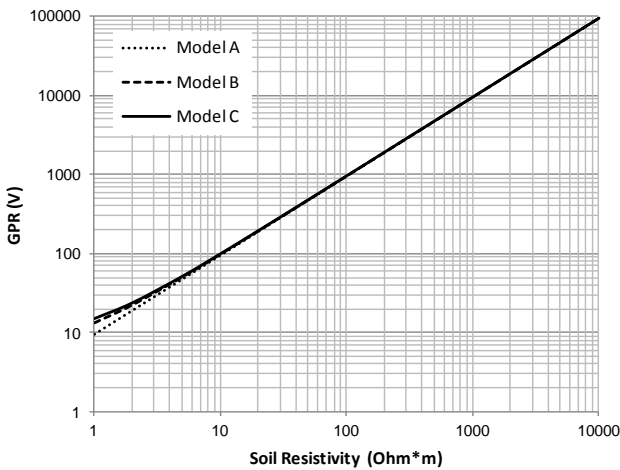
Fig. 3.1. GPR as a function of the soil resistivity - Grid size 50 m x 50 m, mesh size 10 m, 1 kA, 50 Hz.

As expected, the GPR (and then the impedance to earth) increases with the soil resistivity and decreases with the grid size.
Model A results are proportional to the resistivity.
Assuming high resistivity values, B and C models results are also proportional to soil resistivity whereas with low resistivity values, model B results are greater than those of model A because of the self-impedance, and model C results are greater than those of model B due to the mutual

impedance.
In particular, when the soil resistivity is very low, model C results are proportional to the "ρ^c", and (as for [11]), "c=0.40" represents a good estimation.
This phenomenon may be related to the wavelength propagation "λ" in soil.
If "ρ" is high, "λ" is long, the self and mutual impedance effects may be ignored, the electrode may be considered equipotential, and the GPR is mainly related to the self and mutual resistance coefficients which are proportional to "ρ".
Conversely, if "ρ" is low, "λ" is short, the self and mutual impedance effects cannot be ignored, the electrode cannot be considered equipotential, and the GPR is mainly related to the self-impedance.
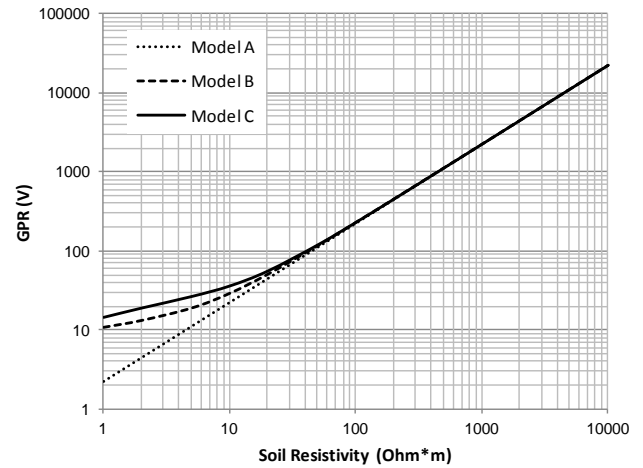
Fig. 3.2. GPR as a function of the soil resistivity - Grid size 200 m x 200 m, mesh size 10 m, 1 kA, 50 Hz.
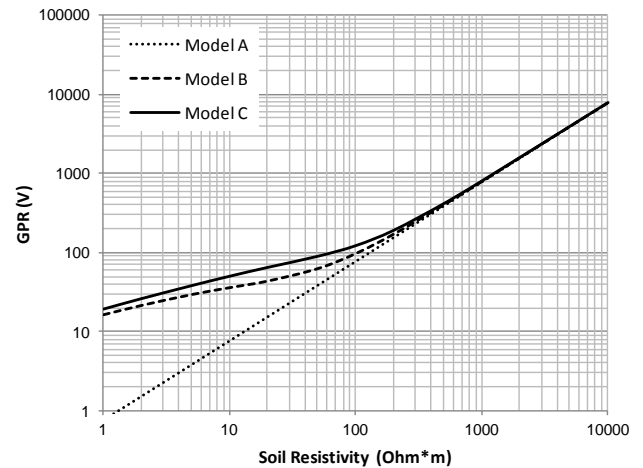
Fig. 3.3. GPR as a function of the soil resistivity - Grid size 600 m x 600 m, mesh size 30 m, 1 kA, 50 Hz.

The self-impedance may be considered as the sum of an internal and an external component. The internal impedance is practically independent of the resistivity of the propagation media. The external impedance with low resistivity propagation media is predominant on the internal one, and may be calculated using approximate formulae (e.g. Sunde or Wedepohl and Wilcox formulae [1], [6]), and with low resistivity, its value is proportional to "$\rho^{0.5}$".
This simple explanation leads to a conclusion which is quite similar to those obtained experimentally.
The differences among the three models' results are more

4

evident as the grid size increases. Fig. 3.4 represents the ratio GPR / GPR model C as a function of the soil resistivity of a grid 600 m x 600 m (this grid has been chosen as example, but the considerations are also valid for the other grid sizes).

Model C has been adopted as a reference because is more accurate than Models A and B and because, as already said, the agreement between this model and other already validated models is excellent.

With reference to the model C results obtained, Fig. 3.4 show that model A gives unacceptable results with low soil resistivity, whereas model B makes a maximum error of about 30% for soil resistivity 20 Ω·m.
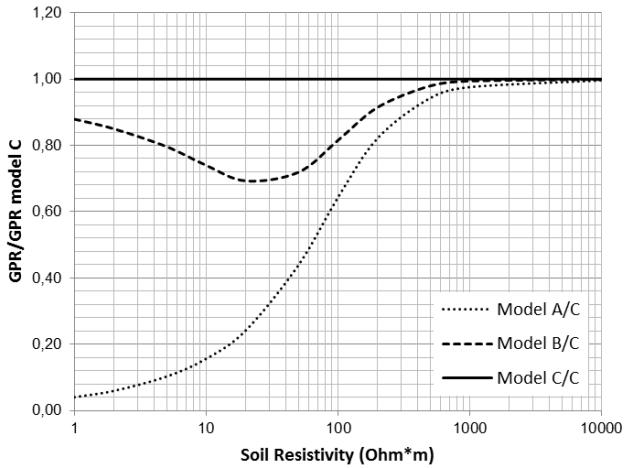
Fig. 3.4. GPR / GPR model C as function of soil resistivity - Grid size 600 m x 600 m.

The difference between B and C models tends to decrease for low and high soil resistivity values. This phenomenon may be explained by considering that the electromagnetic fields' propagation in a dissipative medium takes place according to the propagation coefficient of the medium:

$$\gamma = \sqrt{j\omega\mu(\frac{1}{\rho} + j\omega\varepsilon)} \cong \sqrt{j2\pi\mu \frac{f}{\rho}} \qquad (15)$$

A high soil resistivity value corresponds to the effects of a low frequency, and as understood, at very low frequency, the inductive coupling effects reduce and may be ignored. A low soil resistivity value corresponds to the effects of a high frequency, and as previously established, at a very high frequency, the conductive coupling effects are greater in comparison to the inductive coupling effects because of the strong energy dissipation in the medium.

Now an acceptance criterion for the different models must be adopted.

If we accept an error of 10% on the GPR values with reference to model C results for each grid size, in general, two resistivity values may be found as shown in Fig. 3.4.

With large grids, the error of model B tends to reduce also in the case of low resistivity values and then the condition about the maximum error 10% in general may identifies two resistivity values. This situation is for theoretical interest only, and therefore in these cases the only higher value of resistivity was considered.

By representing the resistivity values set as a function of the grid size, it may be identified the application areas in Fig. 3.5.

In a "log – log" graph, the application limits correspond to straight lines that may be extended by identifying three areas.

All A, B, and C models may be used in the area below the dotted line, whereas B and C models may be adopted in the area between the dotted and dashed lines, and only model C may be adopted above the dashed line.

The model B application area appears to be quite limited.

The solid line indicates a tenth of the wavelength at 50 Hz:

$$\frac{\lambda}{10} \cong 316.2\sqrt{\frac{\rho}{50}} \qquad (16)$$

In summary, at 50 Hz, model C is preferable when "D > λ/10" and, approximately, all A, B, and C models may be adopted when "D < λ/15".

Assuming the current injected in the grid center (and not in the grid corner, as in the previous calculations), the maximum grid size is twice.
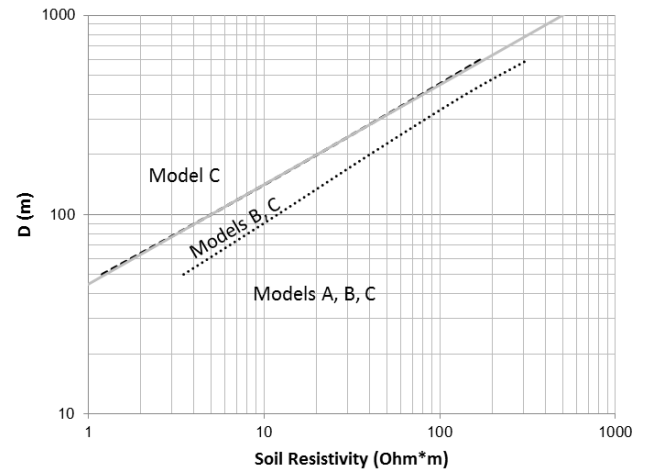
Fig. 3.5. Application limit of the considered models at 50 Hz (Grid size as a function of soil resistivity).

4.   Frequency Analysis

As general rule, it is prudential to establish the frequency of 1 MHz as the application limit of the investigated models. This is because all tested models use the MIM and models B and C use also the SCIM, and the application range of this methods is usually indicated as lower than a few MHz [3] [7] [9]. Both MIM and SCIM may be considered a low frequency approximation of the Sommerfeld integrals (the rigorous solution of the half space problem).

The frequency range 0 – 1 MHz contains all power system frequencies and the most significant frequency of the lightning spectrum.

IEC 62305-1 defined the following standard wave form for lightning currents: first positive stroke 10/350 μs (rise time to peak 10 μs and time to half value 350 μs), first negative stroke 1/200 μs and subsequent stroke 0.25/100 μs. The "equivalent" frequency of the first positive, first negative and subsequent stroke are respectively 25 kHz, 250 kHz and 1 MHz. First positive and negative strokes peak current can reach 200 kA and 100 kA respectively while subsequent stroke can reach 50 kA. Then, the most significant components of the lightning currents are in the frequency range 25 – 250 kHz.

In the following, a uniform soil model with 100 Ω·m resistivity is assumed.

The same five grids of the "Resistivity Analysis" are examined.

As widely known, the relative soil permittivity depends on frequency. Fig. 4.1 shows as an instance the measurement results of the relative permittivity, testing a dry sand sample (with resistivity at least 10 kΩ·m). Regarding this question, the literature is not clear. ITU recommendations [5] indicate that the relative permittivity of ground and water may be considered a constant up to several MHz, and the values are between 3 for very dry ground and about 80 for water. Other literature [13] indicates that relative permittivity of ground varies greatly with frequency.
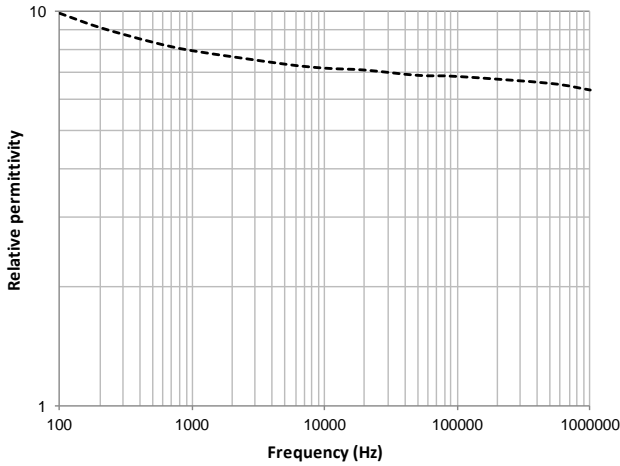
Fig. 4.1. Relative permittivity of dry sand as function of frequency.

Applying the Messier's formulae, for instance, the low frequency relative permittivity could be greater than 10000, whereas at high frequency (several MHz), it tends to an asymptotic value between 4 and 8.

Anyway, soil permittivity is not significant if the following condition is satisfied:

$$\omega\varepsilon << \frac{1}{\rho} \qquad (17)$$

Applying the Messier's formulae with low frequency soil resistivity 100 Ω·m, and high frequency relative permittivity 8, the solution of the previous non linear equation gives about f = 100 kHz. In the frequency range of interests, on this paper, the soil displacement current (related to the soil permittivity) can be neglected or plays a secondary role compared to the conductive current.

In the following, a relative permittivity 1 is taken into account only as an assumption, but this is not crucial for the parametric analysis. In general, a greater relative permittivity corresponds to a lower soil complex resistivity, and then to a lower GPR of the grids.

The frequency is evaluated in the range 1 Hz – 1 MHz (1, 10, 50, 100, 1000, 10000, 100000, 1000000 Hz).

The magnitude of GPR values of very small, medium and very large grids are shown in the following Figures 4.2, 4.3 and 4.4 (dotted line for model A, dashed line for model B, and solid line for model C).
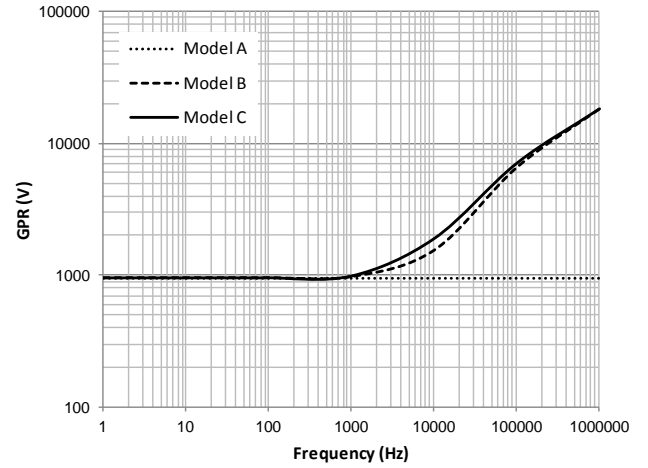
Fig. 4.2. GPR as a function of the frequency - Grid size 50 m x 50 m, mesh size 10 m, 100 Ω·m.
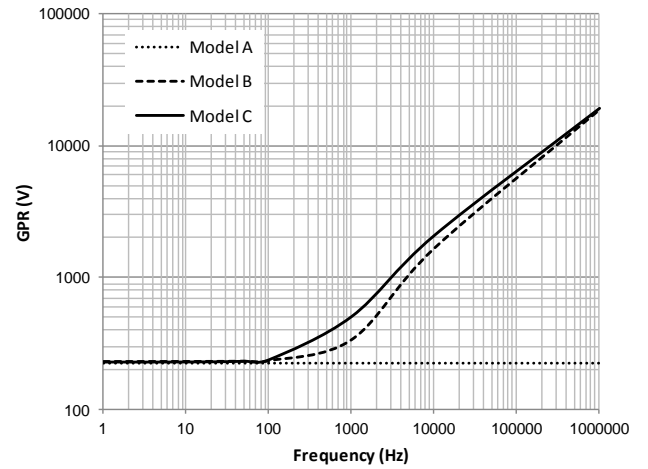
Fig. 4.3. GPR as a function of the frequency - Grid size 200 m x 200 m, mesh size 10 m, 100 Ω·m.
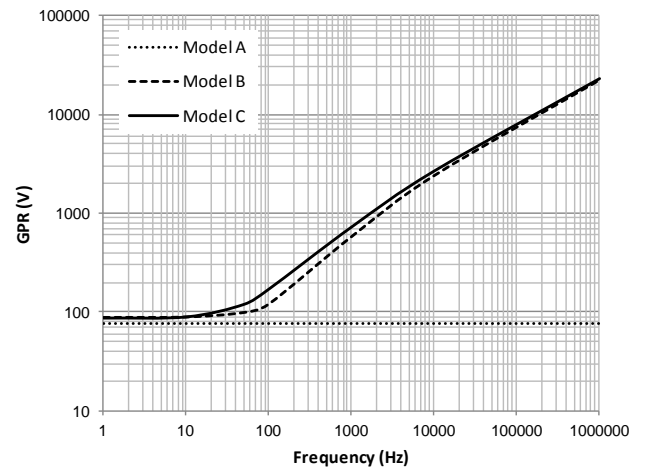
Fig. 4.4. GPR as a function of the frequency - Grid size 600 m x 600 m, mesh size 30 m, 100 Ω·m.

As expected, with the considered soil resistivity value (100 Ω·m) and grid size, the frequency-dependent behavior is inductive for each grid, and using B and C models, GPR rise up with frequency (as known, with high values of soil resistivity and relative permittivity and small electrodes, the frequency-dependent behavior could be resistive or capacitive).

Moreover, as expected, at high frequency (1 MHz), the magnitude of GPR does not depend on the grid size because, due to the voltage drops on self and mutual impedances, the effective part of the grid is limited around the injection point.

In general, two frequency intervals may be identified: a low frequency range where the GPR is frequency-independent and almost equal to the low frequency value, and a high frequency range where the GPR rise up with frequency.

Model A results are frequency-independent.

As anticipated, it exists a correlation between high frequency and low soil resistivity values, and vice versa, between low frequency and high soil resistivity. Then, there is a correlation between soil resistivity and the inverse of frequency.

With high frequency values, model B results are greater than model A results because of the self-impedance, and model C results are greater than model B results because of the mutual impedance.

In particular, when the frequency is high, model C results are proportional to the "f^c", and "c=0.40" represents a good estimation.

The difference among the three models' results is more evident with increasing grid size.

Fig. 4.5 represents the ratio GPR / GPR model C as a function of the frequency for a grid 600 m x 600 m (as an example).

Fig. 4.5 if compared to Fig. 3.4, it makes the correlation quite clear between soil resistivity and the inverse of frequency.
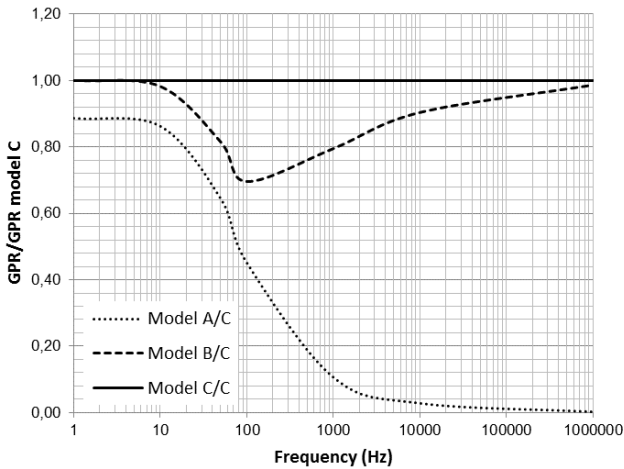
Fig. 4.5. GPR / GPR model C as function of the frequency - Grid size 600 m x 600 m.

With reference to model C results obtained, Fig. 4.5 shows that model A gives unacceptable results when frequency is high, whereas model B makes a maximum error of about 30% for a frequency of about 100 Hz.

A residual difference between model A and B and C models results at low frequency may be attributed to the "dc" resistance component of the self-impedance. When employing a smaller grid, this residual difference tends to disappear.

The correlation between soil resistivity and the inverse of frequency can explain the reason why the difference between B and C models tends to reduce for low and high frequency values.

If we accept an error of 10% on the GPR values with reference to the model C results for each grid size, in general, three frequency values may be found as shown in Fig. 4.5.

Fig. 4.5 shows that the error of model B could also be lower than 10% in the case of high frequency, but this situation is for theoretical interest only, and is therefore not considered.

By representing the frequency values set as a function of the grid size, it may be identified the application areas in Fig. 4.6.
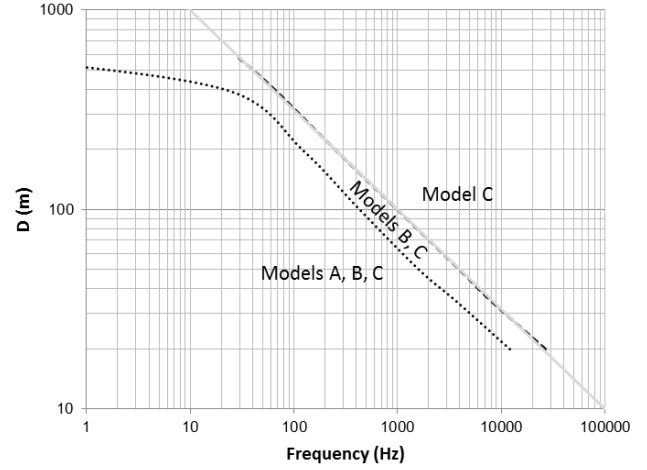
Fig. 4.6. Application limit of the considered models (Grid size as function of frequency).

In a "log – log" graph, the application limits correspond to straight lines that may be extended by identifying three areas.

It is interesting to observe that model A may be used up to 1 MHz with an electrode size smaller than about 10 m (or more if the soil resistivity is greater than 100 Ω·m). This confirms the results published in [12].

A deviation from the straight shape of model A application limit for low frequency may be attributed to the effects of the "dc" component of the self-impedance.

All A, B, and C models may be used in the area below the dotted line, whereas B and C models may be adopted in the area between the dotted and dashed lines, and only model C may be adopted above the dashed line.

The model B application area appears to be quite limited.

The solid line indicates a tenth of the wavelength with 100 Ω·m:

$$\frac{\lambda}{10} \cong 316.2 \sqrt{\frac{100}{f}} \qquad (18)$$

In summary, with soil resistivity of 100 Ω·m, model C is preferable when "D > λ/10", and approximately, all A, B, and C models may be adopted when "D < λ/15".

Moreover, model A may be used with grid size up to 500 m.

5. Discussion and Conclusions

In spite of the extensive literature on the paper subject, there are still no consensus regarding the calculation method that is best suited for grounding system analysis.

The goal of this paper is to provide a possible answer to this open question with a comparison between three calculation models for grounding system analysis based on hybrid methods, MIM and SCIM. Model A takes into account only

the resistive coupling, model B considers also the self-impedance effects, and model C considers both self and mutual impedance effects.

The results of the two parametric soil resistivity and frequency analyses may be resumed into a single graph as in Fig. 5.1, which assumes the unified parameter "ρ/f" (Ω·m/Hz) proportional to the square of the wavelength of propagation in soil.
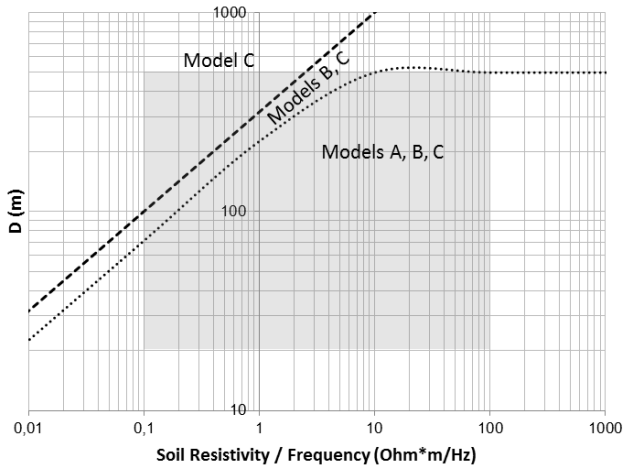
Fig. 5.1. Application limit of the considered models (Grid size as function of the ratio between soil resistivity and frequency).

All A, B, and C models may be used in the area below the dotted line, whereas B and C models may be adopted in the area between the dotted and dashed lines, and only model C may be adopted above the dashed line.

Concerning their application dominion, the GPR calculation errors for each model are lower than 10%.

The highlighted area in Fig. 5.1 indicates the usual condition at 50 Hz, considering 5 Ω·m and 5 kΩ·m respectively as minimum and maximum soil resistivities, and 20 m and 500 m as minimum and maximum grid size.

The final conclusions must be distinguished depending on the frequency.

At power frequency, model A may be used in most practical cases, but it tends to underestimate the results in case of low soil resistivity or large grid sizes. In addition, model A may be used only if the grid size is less than about 500 m due to the effects of "dc" component of the self-impedance. Also, model B tends to underestimate the results in the same condition, and its application area is a little bit more extensive than that of the model A. Model B may be applied to grids with size greater than 500 m only with high soil resistivity.

At high frequency, A and B models may be applied only to small grids.

In general, Model C may be applied in the whole considered range of soil resistivity and frequency.

The parametric analysis are carried out assuming the current injected in a grid corner, conversely, if the injection point is in the grid center, the size limits are twice of those indicated in the Fig. 5.1.

After these conclusions, a question could arise: Why not just use model C?

Model A allows for a reduction in data entry (because it does not require information about the grounding system topology) and computer resources required (memory and computing power), and whenever applicable, it is the preferred model. Model B and model C require the same data entry, but the calculations necessary for model C are more complex and require more computer resources.

If model A cannot be used, and memory and computing power are not limited, model C is the preferred.

Is the opinion of the authors that for frequencies up to a few MHz, model C represents the state-of-the-art and it may be used in order to study the lightning effects taking into account the equivalent frequency of the standard impulse, while model A will continue to remain the reference model for small systems or for preliminary assessments.

Finally, it is important to remember that in this work, the tested grids are composed by copper conductors. Due to copper costs, in some countries grounding systems are often composed by steel conductors. In these cases, the self-impedance values introduce further limits to the application range of the model A, and the model C should be necessary for small systems.

References

[1]   E.D. Sunde, Earth Conduction Effects in Transmission Systems, first ed., D. Van Nostrand Company Inc., New York, 1949.

[2]   S. Ramo, J.R. Whinnery, T. Van Duzer, Fields and Waves in Communication Electronics, first ed., Wiley International Edition, New York and London, 1965.

[3]   ITU / CCITT DIRECTIVES Volume III, Capacitive, inductive and conductive coupling: physical theory and calculation methods, Geneva (1989).

[4]   F.P. Dawalibi, R.D. Southey, Analysis of Electrical Interference from Power Lines to Gas Pipelines – Part I: Computation Methods, IEEE Transactions on Power Delivery, Vol. 4, No. 3, July 1989, pp. 1840 – 1846.

[5]   Recommendation ITU-R P.527-3, Electrical Characteristics of the Surface of the Earth, 1992.

[6]   Electro Magnetic Transient Program Theory Book, Bonneville Power Administration, Portland, Oregon, 1995.

[7]   L.D. Grcev, Computer analysis of Transient Voltages in Large Grounding Systems, IEEE Transactions on Power Delivery, Vol. 11, No. 2, April 1996, pp. 815 – 823.

[8]   R.G. Olsen, M.C. Willis, A comparison of exact and quasi-static methods for evaluating grounding systems at high frequencies, IEEE Transactions on Power Delivery, Vol. 11, No. 2, April 1996, pp. 1071 – 1081.

[9]   R. Andolfato, L. Bernardi, L. Fellin, Aerial and Grounding System Analysis by the Shifting Complex Images Method, IEEE Transactions on Power Delivery, Vol. 15, No. 3, July 2000, pp. 1001 – 1009.

[10]   L.D. Grcev, V. Arnautovski Toseva, Grounding System Modeling for High Frequencies and Transient: Some Fundamental Considerations, IEEE Power Tech Conference Proceedings, Bologna (2003).

[11]   S. Fortin, W. Ruan, F.P. Dawalibi, Comparison of

Computational Methods for the Design and Analysis of Power System Grounding: Parametric Analysis, Power And Energy Systems - IASTED 7th International Conference, USA (2004), pp. 357-363.

[12] J. Meppelink, A. König, Numerische Berechnung der Berührungs- und Schrittspannung (in German), VDE ABB national conference on lightning protection, Germany (2013).

[13] D. Cavka, N. Mora, F. Rachidi, A Comparison of Frequency Dependent Soil Models: Application to the Analysis of Grounding Systems, IEEE Transactions on Electromagnetic Compatibility, Vol. 56, No. 1, February 2014, pp. 177 – 187.

[14] F.H. Silveira, S. Visacro, J. Herrera, H. Torres, Evaluation of lightning-induced voltages over lossy ground by the hybrid electromagnetic model, IEEE Transactions on Electromagnetic Compatibility 51 (1) (2009) 156–160.